

# Oxygen Vacancy-Engineered PEGylated MoO<sub>3-x</sub> Nanoparticles with Superior Sulfite Oxidase Mimetic Activity for Vitamin B1 Detection

Yuan Chen, Tongming Chen, Xiaoju Wu, and Guowei Yang\*

Sulfite oxidase (SuO<sub>x</sub>) is a molybdenum-dependent enzyme that catalyzes the oxidation of sulfite to sulfate to maintain the intracellular levels of sulfite at an appropriate low level. The deficiency of SuO<sub>x</sub> would cause severe neurological damage and infant diseases, which makes SuO<sub>x</sub> of tremendous biomedical importance. Herein, a SuO<sub>x</sub> mimic nanozyme of PEGylated (polyethylene glycol)-MoO<sub>3-x</sub> nanoparticles (P-MoO<sub>3-x</sub> NPs) with abundant oxygen vacancies created by vacancy-engineering is reported. Their level of SuO<sub>x</sub>-like activity is 12 times higher than that of bulk-MoO<sub>3</sub>. It is also established that the superior increased enzyme mimetic activity is due to the introduction of the oxygen vacancies acting as catalytic hotspots, which allows better sulfite capture ability. It is found that vitamin B1 (VB1) inhibits the SuO<sub>x</sub> mimic activity of P-MoO<sub>3-x</sub> NPs through the irreversible cleavage by sulfite and the electrostatic interaction with P-MoO<sub>3-x</sub> NPs. A colorimetric platform is developed for the detection of VB1 with high sensitivity (the low detection limit is 0.46 μg mL<sup>-1</sup>) and good selectivity. These findings pave the way for further investigating the nanozyme which possess intrinsic SuO<sub>x</sub> mimicking activity and is thus a promising candidate for biomedical detection.

## 1. Introduction

Sulfite oxidase (SuO<sub>x</sub>) is a well-known molybdenum-dependent mitochondrial enzyme that catalyzes the oxidation of sulfite to sulfate with the reduction of ferricytochrome C,<sup>[1,2]</sup> which is closely associated with the terminal reaction in the metabolism of sulfur originated from sulfur containing amino acids.<sup>[3-6]</sup> Whereas, human bodies are under a constant threat of being toxified by the excess accumulation of sulfite on account of SuO<sub>x</sub> deficiency,<sup>[7]</sup> leading to severe neurological damage,<sup>[8,9]</sup> attenuated growth of the brain<sup>[6]</sup> and early death in infancy with no effective therapies known.<sup>[5,10]</sup> Therefore, these severe diseases owing to

SuO<sub>x</sub> deficiency which would further compromise the activity of SuO<sub>x</sub>, making SuO<sub>x</sub> of tremendous biomedical importance.


Nevertheless, the use of natural SuO<sub>x</sub> enzymes raise the issues of production and processing costs (such as extraction and purification),<sup>[3,11]</sup> sufficient stability and tolerability of reaction conditions. Nowadays, immense efforts have been taken to investigate the design of SuO<sub>x</sub> alternatives with similar metal center such as some model compounds containing [Mo<sup>VI</sup>O<sub>2</sub>] units<sup>[4,12,13]</sup> or the complexes with [Bu<sub>4</sub>N]<sub>2</sub>[Mo<sup>VI</sup>O<sub>2</sub>(mnt)<sub>2</sub>] (mnt<sup>2-</sup> = 1,2-dicyanoethylenedithiolate)<sup>[14]</sup> as active sites of SuO<sub>x</sub>. However, no model compound or complex which could effectively catalyze the directly physiological substrate like sulfite or bisulfite has been reported for the oxidase-type enzymatic reaction of SuO<sub>x</sub>.<sup>[14,15]</sup> Fortunately, more evident have indicated that MoO<sub>3</sub> nanoparticles with the mimic metal center of SuO<sub>x</sub> could also catalyze the intracellular oxidation of sulfite to sulfate<sup>[4]</sup>

for recovering the SuO<sub>x</sub>-like activity of SuO<sub>x</sub> deficiency cells. However, the bulk MoO<sub>3</sub> was reported with a quite low SuO<sub>x</sub> activity due to its inactive structure which highlighted the importance of introducing nanomaterials with highly active structure.

Vacancy-engineering has been wealthy reported as an effective strategy for promoting the enzyme-mimic activity of nanomaterials.<sup>[16,17]</sup> For instance, the oxygen vacancy sites on the surface of nanocerium leading to the high ratio of Ce<sup>3+</sup>/Ce<sup>4+</sup> which were considered as catalytic hotspots to distinctively enhance the superoxide dismutase (SOD)-like activity.<sup>[18-22]</sup> Meanwhile, similar phenomena could also be observed in CeO<sub>2-x</sub> nanorods with haloperoxidase mimics.<sup>[23,24]</sup> The oxygen vacancies could be occupied with other negatively charged atoms (such as sulfur) that allow better sulfite capture ability.<sup>[23]</sup> Moreover, they are expected to be responsible for the altered redox chemistry of nanomaterials versus bulk materials.<sup>[20-22]</sup> Inspired by the above reported researches, we suggest that the introduction of oxygen vacancies was likely to enhance the SuO<sub>x</sub> activity of MoO<sub>3</sub> nanoparticles. In addition, though the SuO<sub>x</sub> mimic properties of molybdenum oxide were well documented and applied for treating the SuO<sub>x</sub> deficiency,<sup>[4]</sup> their biocatalytic behavior for detecting was virtually unknown.

In this contribution, we demonstrated that PEGylated MoO<sub>3-x</sub> nanoparticles (P-MoO<sub>3-x</sub> NPs) with abundant oxygen vacancies

Y. Chen, T. Chen, X. Wu, Prof. G. Yang  
State Key Laboratory of Optoelectronic Materials and Technologies  
Nanotechnology Research Center  
School of Materials Science & Engineering  
School of Physics  
Sun Yat-sen University  
Guangzhou 510275, Guangdong, P. R. China  
E-mail: stsygw@mail.sysu.edu.cn

 The ORCID identification number(s) for the author(s) of this article can be found under <https://doi.org/10.1002/smll.201903153>.

DOI: 10.1002/smll.201903153

on its surface exhibit an enhanced intrinsic  $\text{SuO}_x$ -like activity versus bulk- $\text{MoO}_3$  (b- $\text{MoO}_3$ ) for catalyzing the oxidation of sulfite to sulfate. Vitamin B1 (VB1) is an essential organic micro-nutrient which is responsible for carbohydrate metabolism in human bodies.<sup>[25,26]</sup> Therefore, understanding the level ranges of VB1 would be a key part for sensing some severe neurological and brain abnormalities, like beriberi and Wernick–Korsakoff syndrome.<sup>[27,28]</sup> Based on the colorimetric reduction reaction of P- $\text{MoO}_{3-x}$  NPs and the hindrance of  $\text{SuO}_x$ -like activity with VB1, a nanoparticles-dependent  $\text{SuO}_x$  mimic sensing platform was established with low-cost, high sensitivity, and good selectivity for detecting the VB1. We also confirmed that the sensing mechanism involves the attenuation in  $\text{SuO}_x$ -like activity of P- $\text{MoO}_{3-x}$  NPs upon the addition of VB1. In addition, the hindrance of  $\text{SuO}_x$  activity was mainly induced by the irreversible cleavage of VB1 in the presence of sulfite<sup>[29]</sup> and the electrostatic interaction between VB1 and P- $\text{MoO}_{3-x}$  NPs. Thus, these results make P- $\text{MoO}_{3-x}$  NPs with the intrinsic  $\text{SuO}_x$  mimic activity a candidate for potential utilizing in biosensing.

## 2. Results and Discussion

The hydrophilic P- $\text{MoO}_{3-x}$  NPs were prepared by following a hydrothermal process reported earlier,<sup>[30]</sup> and the proposed process is schematically illustrated in **Figure 1a**. Under the addition

of ethanol and PEG-4000 and the modification with hydrochloric acid resulted in vacancy-engineered  $\text{MoO}_{3-x}$  NPs. Transmission electron microscope (TEM) (**Figure 1b**) and magnified high resolution transmission electron microscope (HRTEM) (**Figure 1c**) images reveal that the as-prepared P- $\text{MoO}_{3-x}$  were particles-like with 0.209 nm lattice fringe spacing corresponding to the  $d$ -spacing of (222) plane. Meanwhile, the diameter of the particle structure was ranged from 5 to 14 nm (**Figure 1e**). Moreover, the presence of some vacancies as hot-spots exist on the surface of P- $\text{MoO}_{3-x}$  NPs can be observed through the false color image of HETEM<sup>[19,31]</sup> in **Figure 1d**. Furthermore, scanning electron microscopy (SEM) (**Figure 1f**) and atomic force microscope (AFM) (**Figure 1g**) images confirm that P- $\text{MoO}_{3-x}$  was formed with regular particles structure with a thickness of 31.25 nm (**Figure S1**, Supporting Information), which were in line with the TEM results.

To further explore the structure characteristics, X-ray powder diffraction (XRD) was carried out to obtain the crystalline phase of P- $\text{MoO}_{3-x}$  NPs. Through the XRD pattern in **Figure 2a**, the diffraction peaks could be identified as the mixture of orthorhombic  $\text{Mo}_4\text{O}_{11}$  phase (JCPDS 65-0397, marked with ♣) and monoclinic  $\text{MoO}_2$  phase (JCPDS 65-1273, marked with ♥).<sup>[30]</sup> Meanwhile, the elemental mapping and corresponding energy dispersive X-ray spectroscopy (EDS) analysis results (**Figure S2**, Supporting Information) reveal that Mo and O elements are uniformly distributed on the surface of P- $\text{MoO}_{3-x}$

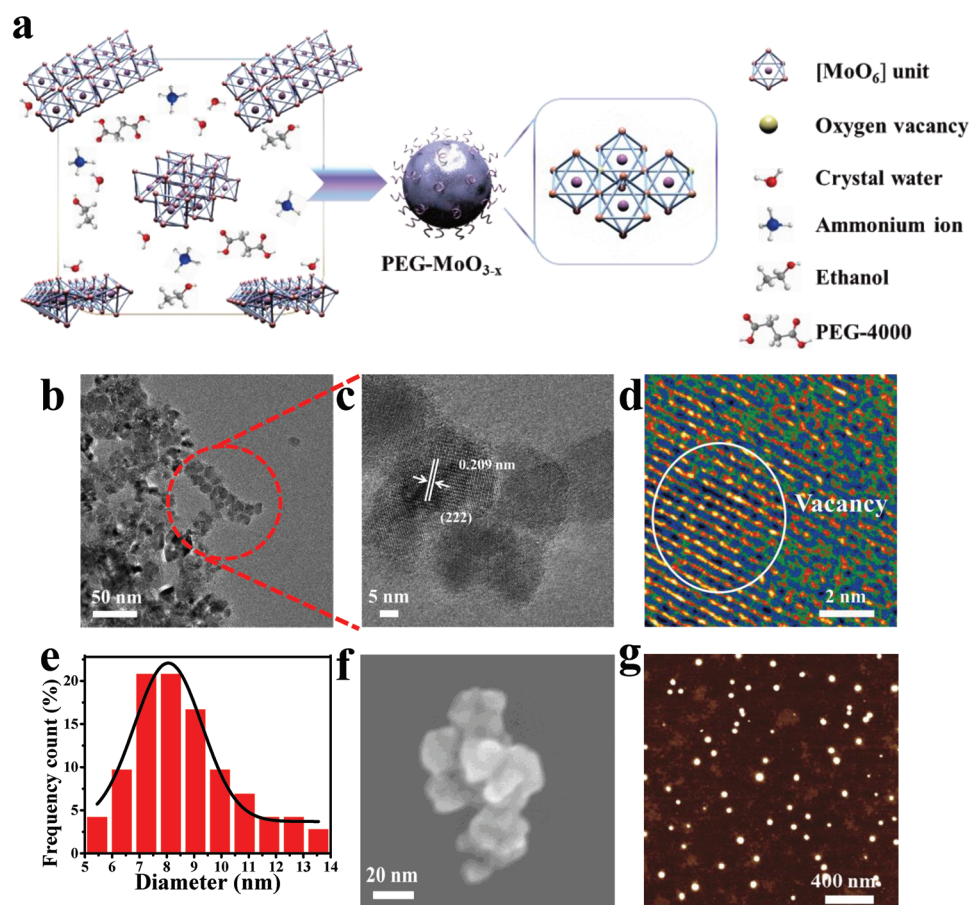


**Figure 1.** a) Schematic illustration of the formation of vacancy engineered P- $\text{MoO}_{3-x}$  NPs. b,c) Low-magnification TEM and HRTEM images. d) False-color image of HRTEM image. e) Size distributions of P- $\text{MoO}_{3-x}$  NPs corresponding to TEM images. f) SEM image. g) AFM image.

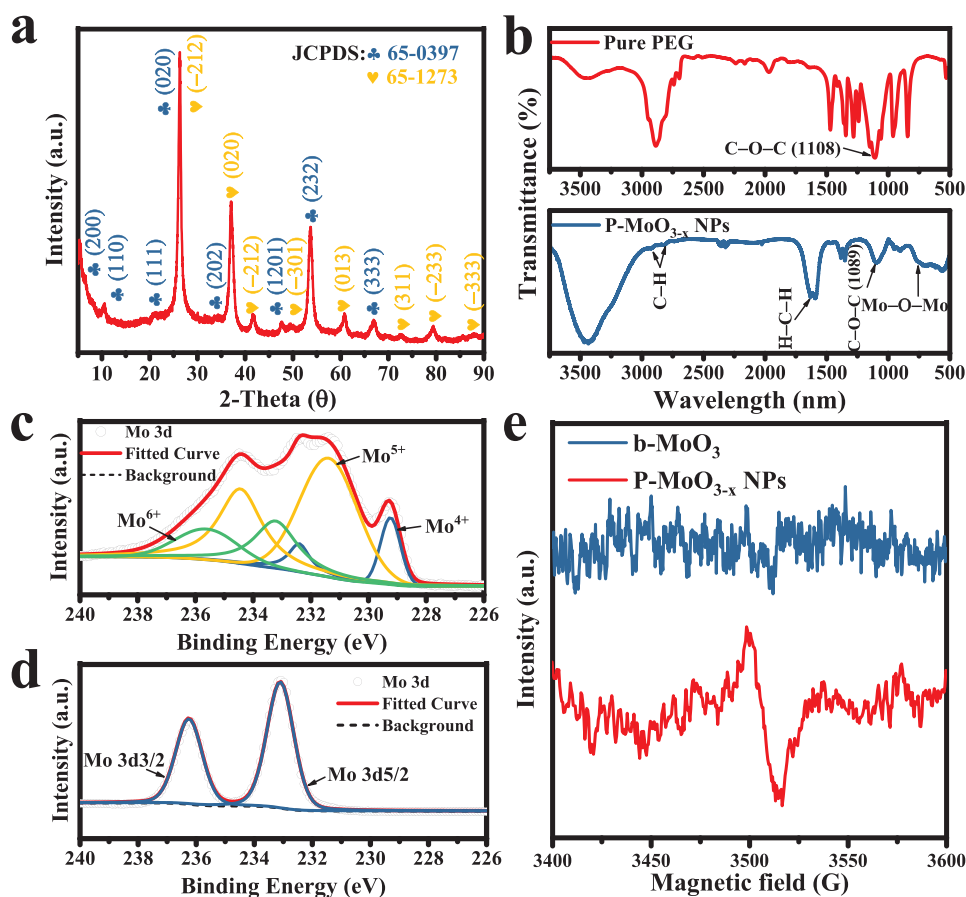


**Figure 2.** a) XRD pattern of P-MoO<sub>3-x</sub> NPs. b) FTIR spectra of P-MoO<sub>3-x</sub> NPs and pure PEG. c) XPS spectra of P-MoO<sub>3-x</sub> NPs and b-MoO<sub>3</sub> respectively. d) ESR spectra of P-MoO<sub>3-x</sub> NPs and b-MoO<sub>3</sub>.

NPs, along with C element derived from PEG-4000. Moreover, no other elements could be detected attributing to the EDS analysis, reveals the high purity of the as-prepared P-MoO<sub>3-x</sub> NPs.

Furthermore, to confirm the successful synthesis of P-MoO<sub>3-x</sub> NPs, Fourier transform infrared (FTIR) spectra (Figure 2b) was performed. In details, the peak located at 753 cm<sup>-1</sup> can be contributed to stretching vibration of Mo–O–Mo.<sup>[32]</sup> The peaks at 2929 and 2853 cm<sup>-1</sup> are assigned to the asymmetric and symmetric stretching vibration of –CH<sub>2</sub>– groups in PEG,<sup>[30]</sup> respectively. Meanwhile, the stretching vibration of C–O–C group at 1108 cm<sup>-1</sup> in pure PEG shifted to a lower wave number compared with P-MoO<sub>3-x</sub> NPs, confirming that PEG has been successfully functionalized on the surface of P-MoO<sub>3-x</sub> NPs.

In addition, it has been reported that PEG was introduced as a stabilizer to prevent MoO<sub>3-x</sub> NPs from agglomeration and then endowed them with hydrophilic surface. Moreover, both of the chemical reduction (such as PEG,<sup>[30,32]</sup> PVP,<sup>[33]</sup> glycine,<sup>[34]</sup> chitosan,<sup>[35]</sup> and hyaluronic acid<sup>[34]</sup>) or thermal annealing (PDDA)<sup>[36,37]</sup> were reported to cause the structure disorder, and bring about the formation of oxygen vacancies on the surface of molybdenum oxides. PEG was also acted as a reduction agent to inhibit the growth of crystal and modulating the chemical states (Figure S3, Supporting Information).<sup>[32]</sup> The texture properties

of P-MoO<sub>3-x</sub> NPs and b-MoO<sub>3</sub> free of PEG were compared via nitrogen absorption and desorption isotherm measurements (Figure S4a,c, Supporting Information). The Brunauer–Emmett–Teller (BET) specific surface areas of P-MoO<sub>3-x</sub> NPs and b-MoO<sub>3</sub> were 79.22 and 18.70 m<sup>2</sup> g<sup>-1</sup>, respectively (Table S1, Supporting Information). Whereas both of the samples have the similar center pore diameter at 2.10/2.53 nm from the BJH pore size distributions (Figure S4b,d, Supporting Information), P-MoO<sub>3-x</sub> NPs possess more abundant pores in the range of 2–40 nm. These results confirmed that the introduction of oxygen vacancies through PEGylating would effectively increase the specific surface area of molybdenum oxides without causing lattice collapse in the framework. And it has also been proved by Pettes and co-workers<sup>[36,37]</sup> and Tang and co-workers.<sup>[38]</sup> Moreover, it was predicted that eliminating ions and creating defects in the materials could effectively decreased the large surface energy of nanoparticles.<sup>[19]</sup> To attain low energy systems through removing oxygen atoms results in the reduction of adjacent metal ions.<sup>[18]</sup> In compare with the b-MoO<sub>3</sub>, the obtained P-MoO<sub>3-x</sub> NPs exhibit a distinct dark blue color (Figure S5, Supporting Information), suggesting the presence of low-valence Mo in the samples.<sup>[35]</sup> The presence of oxygen vacancies in P-MoO<sub>3-x</sub> NPs were further demonstrated by electron spin resonance (ESR) solid powder analysis (Figure 2e). In P-MoO<sub>3-x</sub> NPs, a distinct Lorentzian line with g value about 2.0 that

corresponding to the unpaired electrons<sup>[38–40]</sup> can be observed, confirming oxygen vacancies were formed in P-MoO<sub>3-x</sub> NPs. In contrast, no obvious ESR signal can be detected for b-MoO<sub>3</sub>, suggesting the disappearance of oxygen vacancies. For careful determining the degree of reduction and the surface chemical environment of P-MoO<sub>3-x</sub> NPs, thermal gravimetric (TGA) and X-ray photoelectron spectroscopy (XPS) analysis were characterized, respectively. The oxygen vacancy concentration could be estimated by TGA. In general, shown in Figure S6 in the Supporting Information, the reduced oxides show a lower mass loss with TGA when heated in the air rather than in nitrogen.<sup>[41]</sup> From the TGA calculations, the composition of P-MoO<sub>3-x</sub> NPs and b-MoO<sub>3</sub> were estimated to MoO<sub>1.61</sub> and MoO<sub>2.95</sub> (Table S3, Supporting Information), respectively. Thus, these results suggested that P-MoO<sub>3-x</sub> NPs may achieve with an “imperfect” structure. Besides, the presence of vacancies in P-MoO<sub>3-x</sub> NPs may be attributed to the surface oxygen atoms removing. Meanwhile, the remarkable reduction of MoO<sub>3</sub> in the presence of PEG from TGA analyses demonstrated that PEGylation significantly boosted the oxygen stoichiometry concentrations of molybdenum oxides. Moreover, in order to quantify the oxidation states of samples, XPS analysis was employed. For comparison, b-MoO<sub>3</sub> was also examined. As shown in Figure S7 in the Supporting Information, only Mo, O, and C elements can be detected from both samples which are in good agreement with EDS results. Compared with b-MoO<sub>3</sub>, the O 1s level (Figure S8, Supporting Information) of P-MoO<sub>3-x</sub> NPs show a shift of 0.18 eV to a low binding energy, suggesting the low-coordination O atoms in the structure of P-MoO<sub>3-x</sub> NPs.<sup>[31]</sup> Meanwhile, the peaks at 530.18 and 531.4 eV contribute to the bridging oxygen of Mo–O–Mo and oxygen atoms nearby the oxygen vacancies, respectively.<sup>[34]</sup> These results reveal the existence of O vacancies in P-MoO<sub>3-x</sub> NPs rather in b-MoO<sub>3</sub>. Furthermore, the high-resolution XPS spectrum of Mo 3d of P-MoO<sub>3-x</sub> NPs (Figure 2c) could be divided into six peaks. The weak peaks located at 229.3 and 232.5 eV are assigned to 3d<sub>5/2</sub> and 3d<sub>3/2</sub> of Mo<sup>4+</sup>.<sup>[42]</sup> The main peaks at 231.4 and 234.5 eV contribute to 3d<sub>5/2</sub> and 3d<sub>3/2</sub> of Mo<sup>5+</sup>.<sup>[43]</sup> In addition, the peaks observed at 233.18 and 235.68 eV represent the Mo 3d<sub>5/2</sub> and 3d<sub>3/2</sub> of Mo<sup>6+</sup>.<sup>[30,32]</sup> While, only Mo<sup>6+</sup> peaks (233.09, 236.24 eV) could be detected in b-MoO<sub>3</sub> for comparison (Figure 2d), and the two peaks shifted to a higher binding energy over than that of P-MoO<sub>3-x</sub> NPs, which further indicating the loss of O atoms results in the reduction of adjacent of Mo atoms. And the amount of Mo<sup>4+</sup>, Mo<sup>5+</sup>, and Mo<sup>6+</sup> of P-MoO<sub>3-x</sub> NPs according to statistical analysis for peaks areas was estimated to be around 12.9%, 64.1%, and 23.0%. Mo<sup>4+</sup>/Mo<sup>6+</sup> and Mo<sup>5+</sup>/Mo<sup>6+</sup> for P-MoO<sub>3-x</sub> NPs were calculated as 0.56 and 2.79, demonstrating that its oxygen vacancy sites consisted surface. Besides, integrated with the X-ray fluorescence spectroscopy (XRF) analysis (the O/Mo atomic ratio of P-MoO<sub>3-x</sub> NPs was calculated as 1.95, shown in Table S2 in the Supporting Information), it indicated that molybdenum oxides formed with oxygen vacancies, which is agreed with XRD and TGA results.

The above results reveal that the PEGylated MoO<sub>3-x</sub> NPs with oxygen vacancies have been successfully prepared.

To characterize the SuO<sub>x</sub>-like activity of P-MoO<sub>3-x</sub> NPs, A colorimetric approach using K<sub>3</sub>[Fe (CN)<sub>6</sub>] as electron acceptor in order to exclude possible side reactions of natural electron

acceptor cytochrome C<sup>[4,5,44]</sup> was carried out by measuring the reduction rate at 420 nm. As shown in Figure S9 in the Supporting Information which demonstrated the ΔAbsorbance (A<sub>0</sub>–A) variation of different systems at 420 nm, P-MoO<sub>3-x</sub> NPs could effectively catalyze SO<sub>3</sub><sup>2-</sup> resulting in the reduction of [Fe (CN)<sub>6</sub>]<sup>3-</sup>. In addition, comparing with the control experiment without P-MoO<sub>3-x</sub> NPs in the same intervals, the reduction evolution of P-MoO<sub>3-x</sub> NPs–SO<sub>3</sub><sup>2-</sup>–[Fe (CN)<sub>6</sub>]<sup>3-</sup> system varied quickest, and the ΔAbsorbance slope at 420 nm was the highest. Accordingly, this distinctive ΔAbsorbance variation at 420 nm indicated the intrinsic SuO<sub>x</sub>-like activity of P-MoO<sub>3-x</sub> NPs.

To further investigate the SuO<sub>x</sub>-like activity of P-MoO<sub>3-x</sub> NPs, apparent steady-state kinetic for the reaction was employed. Within the range of sulfite (0.0–1.5 × 10<sup>-3</sup> M) while fixing the concentrations of P-MoO<sub>3-x</sub> NPs (50 μg mL<sup>-1</sup>) and K<sub>3</sub>[Fe (CN)<sub>6</sub>] (0.3 × 10<sup>-3</sup> M), a typical Michaelis–Menton curve towards sulfite can be observed (Figure 3a), which is consistent with that reported for the native SuO<sub>x</sub>.<sup>[11,14,45]</sup> Meanwhile, when varied the concentration of K<sub>3</sub>[Fe (CN)<sub>6</sub>] (0.0–0.6 × 10<sup>-3</sup> M) with fixed concentrations of P-MoO<sub>3-x</sub> NPs (50 μg mL<sup>-1</sup>) and sulfite (0.66 × 10<sup>-3</sup> M) vice versa, a similar curve possesses linear dependence behavior with no cooperative can be observed in Figure 3b. This result suggested that K<sub>3</sub>[Fe (CN)<sub>6</sub>] stabilizes the inactive Mo<sup>IV</sup> oxidation state.<sup>[4,44]</sup> Moreover, to investigate the relationship between sulfite and K<sub>3</sub>[Fe (CN)<sub>6</sub>] in the reaction, the SuO<sub>x</sub>-like activity of P-MoO<sub>3-x</sub> NPs (50 μg mL<sup>-1</sup>) over a range of sulfite and K<sub>3</sub>[Fe (CN)<sub>6</sub>] concentrations was measured in Figure 3c,d, respectively. Double reciprocal plots of initial velocity versus sulfite or K<sub>3</sub>[Fe (CN)<sub>6</sub>] can be obtained for a range of concentrations of each other. In addition, the obtained lines in an approximately linear manner fit the typical ping-pong mechanism, as is founded for hepatic SuO<sub>x</sub>.<sup>[11]</sup> These results indicate that the P-MoO<sub>3-x</sub> NPs bind and react with the first substrate, releasing the first product before reacting with the second substrate.<sup>[46,47]</sup>

Beyond that, Figure 3e offered a proposal mechanism of SuO<sub>x</sub>-like activity of P-MoO<sub>3-x</sub> NPs in the presence of sulfite and K<sub>3</sub>[Fe (CN)<sub>6</sub>] which including steps of sulfite binding, two electron oxidative hydroxylation to produce sulfate, two successive intramolecular one-electron transfers to the Mo<sup>V</sup> intermediate with the reduction of intermolecular electron acceptor.<sup>[1,4,14,44,45]</sup> Nevertheless, no Mo<sup>V</sup> intermediate ESR signal can be detected in the Moco-containing Arsenite oxidase from *Alcaligenes faealis*, nor of the reaction in the presence of P-MoO<sub>3-x</sub> NPs (50 μg mL<sup>-1</sup>) with sulfite (0.66 × 10<sup>-3</sup> M) and K<sub>3</sub>[Fe (CN)<sub>6</sub>] (0.3 × 10<sup>-3</sup> M) in Figure S10 in the Supporting Information. Since the reduction or the oxidation of the active site occurs without the accumulation of Mo<sup>V</sup> which also indicates the absence of Mo<sup>V</sup> ESR signal derives from the obligate two-electron center.<sup>[48]</sup>

Besides, to confirm that P-MoO<sub>3-x</sub> NPs could promote the formation of sulfate, BaCl<sub>2</sub> (8.5 × 10<sup>-3</sup> M) was added in the solution which was prepared by incubation P-MoO<sub>3-x</sub> NPs (50 μg mL<sup>-1</sup>) with sulfite (0.66 × 10<sup>-3</sup> M) and cytochrome C (0.1 mg mL<sup>-1</sup>) for 1 h in the dark. The obtained precipitate with white color was compared with standard BaSO<sub>4</sub> by IR analysis. As shown in Figure S11 in the Supporting Information, the peaks of the precipitate at 1065 and 609 cm<sup>-1</sup> are assigned to the stretching

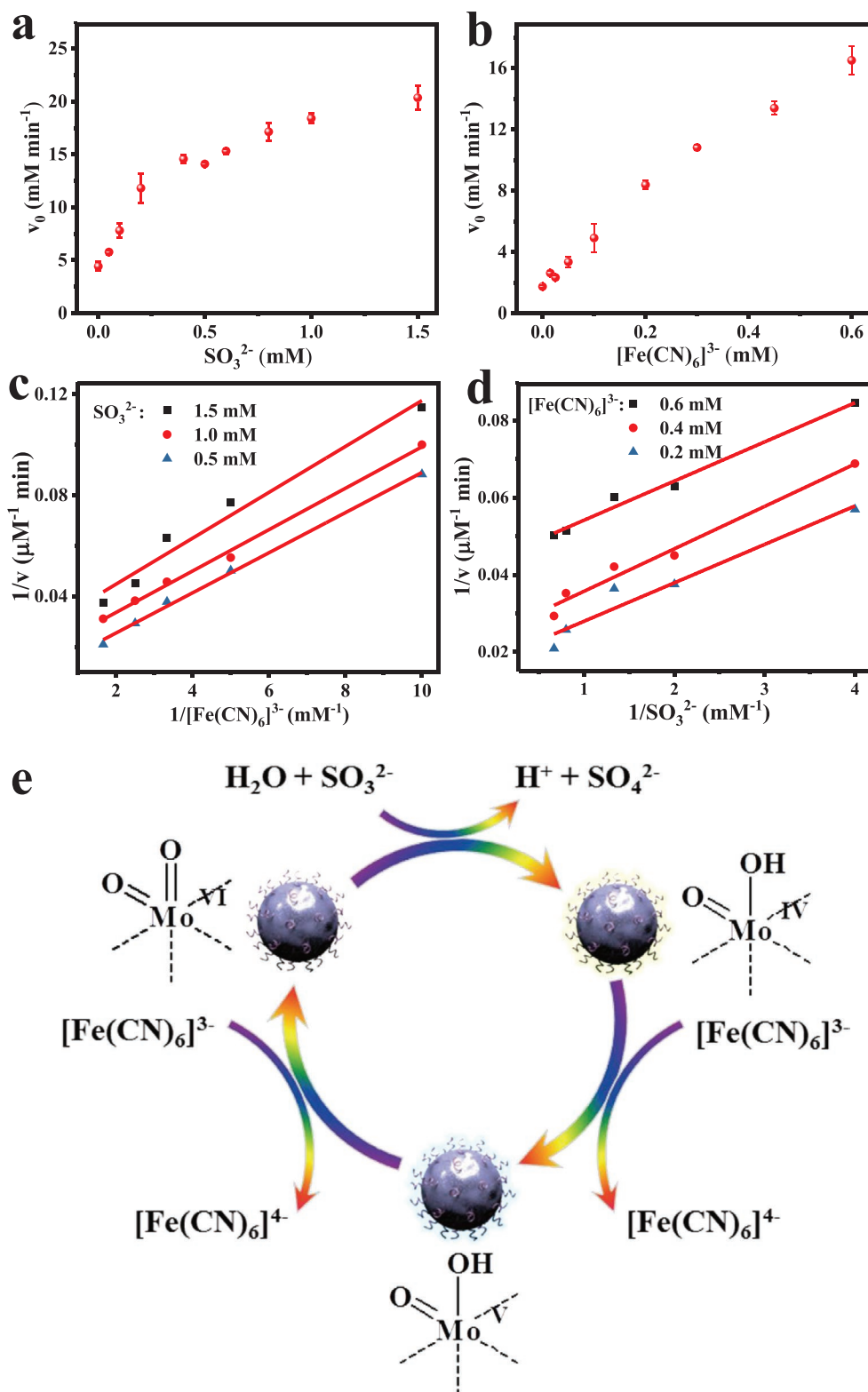


**Figure 3.** Apparent steady-state kinetic assay and SuO<sub>x</sub>-like catalytic mechanism of P-MoO<sub>3-x</sub> NPs. Concentration dependence study of P-MoO<sub>3-x</sub> NPs in the presence of P-MoO<sub>3-x</sub> NPs (0.05 mg mL<sup>-1</sup>). a) The concentration of K<sub>3</sub>[Fe(CN)<sub>6</sub>] was 0.3 × 10<sup>-3</sup> M and the sulfite concentration was varied from 0 to 1.5 × 10<sup>-3</sup> M. b) The concentration of sulfite was 0.66 × 10<sup>-3</sup> M while the concentration of K<sub>3</sub>[Fe(CN)<sub>6</sub>] was varied from 0 to 0.6 × 10<sup>-3</sup> M. c,d) Double-reciprocal plots of P-MoO<sub>3-x</sub> NPs at a fixed initial concentration of one substrate while varying concentration of the other substrate for sulfite and K<sub>3</sub>[Fe(CN)<sub>6</sub>]. The error bars represent the standard deviation of three measurements. (4) The proposed SuO<sub>x</sub> mimic mechanism of P-MoO<sub>3-x</sub> NPs.

vibration of S–O groups in standard BaSO<sub>4</sub>, which further demonstrates that P-MoO<sub>3-x</sub> NPs mediated the formation of sulfate.

Meanwhile, the kinetic parameters of SuO<sub>x</sub>-like activity of P-MoO<sub>3-x</sub> NPs were measured based on the Michaelis–Menton model and Lineweaver–Burk equation,<sup>[46,49,50]</sup> and the results were listed in Table S3 in the Supporting Information. P-MoO<sub>3-x</sub> NPs have a higher K<sub>m</sub> (0.12 × 10<sup>-3</sup> M) value towards sulfite than human SuO<sub>x</sub> (K<sub>m</sub> (SO<sub>3</sub><sup>2-</sup>) = 0.017 × 10<sup>-3</sup> M),<sup>[6]</sup> demonstrating its lower affinity for sulfite as substrate. However, the K<sub>m</sub> (SO<sub>3</sub><sup>2-</sup>) of P-MoO<sub>3-x</sub> NPs was significantly lower than many reported native or artificial SuO<sub>x</sub>, such as human SuO<sub>x</sub> mutant R160Q (K<sub>m</sub> (SO<sub>3</sub><sup>2-</sup>) = 0.17 × 10<sup>-3</sup> M), goat SuO<sub>x</sub> (K<sub>m</sub> (SO<sub>3</sub><sup>2-</sup>) = 0.7 × 10<sup>-3</sup> M) and

MoO<sub>3</sub>-TPP (K<sub>m</sub> (SO<sub>3</sub><sup>2-</sup>) = 0.59 ± 0.02 × 10<sup>-3</sup> M),<sup>[4,6,48]</sup> suggesting its higher affinity towards sulfite.

Moreover, along with the increase concentration of P-MoO<sub>3-x</sub> NPs with a fixed concentration of sulfite (0.66 × 10<sup>-3</sup> M), the reduction rate of K<sub>3</sub>[Fe (CN)<sub>6</sub>] exhibits a linear-dependence behavior. Nevertheless, the reduction rate of K<sub>3</sub>[Fe (CN)<sub>6</sub>] obvious reduces in the presence of b-MoO<sub>3</sub> in Figure 4a and Figure S12 in the Supporting Information, confirming the enhanced SuO<sub>x</sub>-like activity of P-MoO<sub>3-x</sub> NPs. At a same concentration, P-MoO<sub>3-x</sub> NPs exhibited a level of activity 12 times higher than bulk-MoO<sub>3</sub>, the significantly higher activity of P-MoO<sub>3-x</sub> NPs may be derived from its hydrophilic surface, higher surface area, and vacancy-engineered structure.

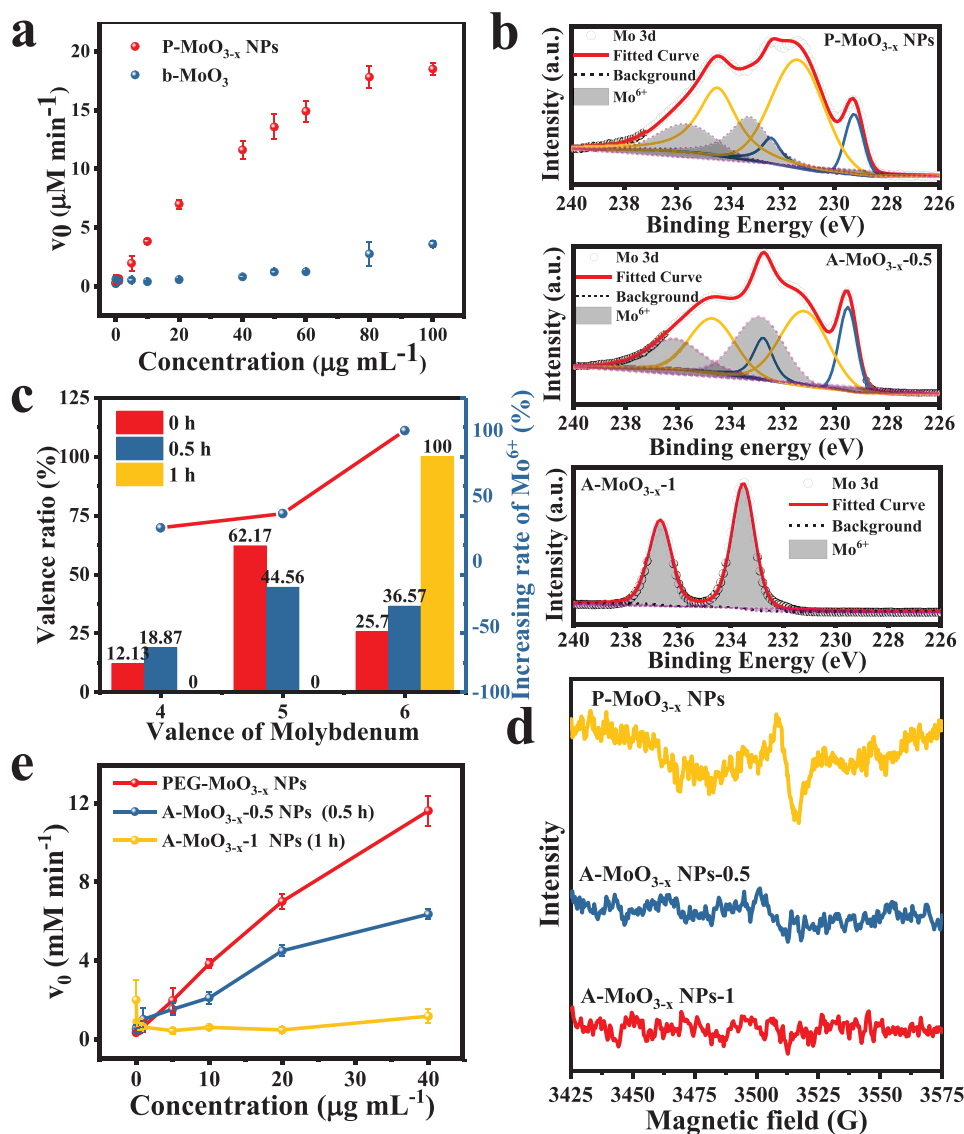


**Figure 4.** Mechanism of the enhanced SuO<sub>x</sub>-like activity of P-MoO<sub>3-x</sub> NPs through vacancy-engineering. The concentrations of sulfite and K<sub>3</sub>[Fe (CN)<sub>6</sub>] in the assay were 0.66 and 0.3 × 10<sup>-3</sup> M, respectively. a) Comparison of the SuO<sub>x</sub>-like activity of P-MoO<sub>3-x</sub> NPs and b-MoO<sub>3</sub> at the same concentration. b) The Mo 3d core level spectra of P-MoO<sub>3-x</sub> NPs and surface modified-P-MoO<sub>3-x</sub> NPs through air-annealing at 400 °C for 0.5 and 1 h, labeled as A-MoO<sub>3-x-0.5</sub> and A-MoO<sub>3-x-1</sub>. c) The valence ratio and Mo<sup>6+</sup> increasing rates of P-MoO<sub>3-x</sub> NPs, A-MoO<sub>3-x-0.5</sub>, and A-MoO<sub>3-x-1</sub>. d) ESR spectra of P-MoO<sub>3-x</sub> NPs, A-MoO<sub>3-x-0.5</sub>, and A-MoO<sub>3-x-1</sub>. e) Comparison of the SuO<sub>x</sub>-like activity of P-MoO<sub>3-x</sub> NPs, A-MoO<sub>3-x-0.5</sub>, and A-MoO<sub>3-x-1</sub> at the same concentration.

Generally, the enzymatic reactions confined on surface or at the interfaces of the nanomaterials are considered to be more efficient.<sup>[51]</sup> The hydrophilic chains of PEG render P-MoO<sub>3-x</sub> NPs with high hydrophilicity.<sup>[52]</sup> And the hydrophilic surface facilitates particle mobility in the solution and endows them from agglomeration. Therefore, it makes P-MoO<sub>3-x</sub> NPs easier to bind with substrates. The hydrophilicity of P-MoO<sub>3-x</sub> NPs can be evaluated via measuring the contact angle. As shown in Figure S13 in the Supporting Information, the contact angle between water and glass substrate was 45.1°, while decreased to 33.5° with b-MoO<sub>3</sub> coated glass substrate. Moreover, when the substrate was substituted by P-MoO<sub>3-x</sub> NPs coated glass substrate, the contact angle significantly dropped to 10.1°. Besides, by comparison the BET results of P-MoO<sub>3-x</sub> NPs with b-MoO<sub>3</sub>, P-MoO<sub>3-x</sub> NPs possess higher specific surface area and more abundant pores (Table S1 and Figure S1, Supporting Information), which could improve the oxygen diffusion to the surface of P-MoO<sub>3-x</sub> NPs. These results indicate the incredibly hydrophilicity and higher surface area effects of P-MoO<sub>3-x</sub> NPs compared with b-MoO<sub>3</sub> which is in line with the SuO<sub>x</sub>-like activity performance.

Meanwhile, P-MoO<sub>3-x</sub> NPs with abundant oxygen vacancies which could be occupied with electronegatively charged sulfur atoms allow better sulfite capture ability.<sup>[23]</sup> In addition, P-MoO<sub>3-x</sub> NPs have surface with molybdenum ions with multiple oxidation states (Mo<sup>4+</sup>, Mo<sup>5+</sup>, and Mo<sup>6+</sup>) which were induced by oxygen vacancies. Those exposed ions and oxygen vacancies are regarded as catalytic hotspots which are vital to capture the substrate (sulfite) and activate them at the active sites.<sup>[19]</sup>

Therefore, to rule out that the enhanced SuO<sub>x</sub>-like activity of P-MoO<sub>3-x</sub> NPs derived from the vacancy-engineered structure, the SuO<sub>x</sub>-like activity of P-MoO<sub>3-x</sub> NPs after surface modifying was measured. In this case, P-MoO<sub>3-x</sub> NPs were air-annealed in different time (0.5 h, 1 h, labeled as A-MoO<sub>3-x-0.5</sub> and A-MoO<sub>3-x-1</sub>) to oxidize the amount of low valence states of molybdenum ions (Mo<sup>4+</sup> and Mo<sup>5+</sup>) to Mo<sup>6+</sup>. As shown in Figure S6 and Table S4 in the Supporting Information, the composition of A-MoO<sub>3-x-0.5</sub> and A-MoO<sub>3-x-1</sub> was calculated as MoO<sub>2.94</sub> and MoO<sub>2.99</sub> by TGA analysis, demonstrating the degree of reduction decreased with the increase of annealing time. In addition, comparing with P-MoO<sub>3-x</sub> NPs free of air-annealing, the O1s (Figure S14, Supporting Information) of A-MoO<sub>3-x-0.5</sub> and A-MoO<sub>3-x-1</sub> shown a shift of 0.33 and 0.47 eV to a high binding energy, respectively. Moreover, along with increasing the air-annealed time, the content of Mo<sup>6+</sup> (Figure 4b,c) was gradually increased, suggesting the occurrence of high-temperature repairing for defect sites.<sup>[53]</sup> In addition, the ESR signals of unpaired electrons also exhibit a declining trend in Figure 4d, confirming the disappearance of vacancies. Besides, the SuO<sub>x</sub>-like activity of A-MoO<sub>3-x</sub> NPs was significantly reduced as the removal of the vacancies (Figure 4e). While no new crystalline phase could be observed from A-MoO<sub>3-x-0.5</sub> or A-MoO<sub>3-x-1</sub> after air-annealing (Figure S15a, Supporting Information). Meanwhile, A-MoO<sub>3-x-0.5</sub> and A-MoO<sub>3-x-1</sub> also maintained a similar nanoparticle-like morphology (Figure S15b,c, Supporting Information). Integrate with the decreasing SuO<sub>x</sub>-like activity of A-MoO<sub>3-x-0.5</sub> and A-MoO<sub>3-x-1</sub>, the above results also proved that the SuO<sub>x</sub>-like reaction mainly occurs on the surface of the catalyst. In addition,

oxygen vacancies on the surface of molybdenum oxides play an important role in the SuO<sub>x</sub>-like reaction.

The decline in performance of A-MoO<sub>3-x-0.5</sub> and A-MoO<sub>3-x-1</sub> can be assign to the following factors. With the occurrence of high-temperature repairing for defect sites (removal the oxygen vacancies), the intensity of monoclinic MoO<sub>2</sub> phase was generally decreased (Figure S15a, Supporting Information). The decline in the intensity of monoclinic MoO<sub>2</sub> could effectively inhibit the electron transfer through the core of the P-MoO<sub>3-x</sub>, which has also been proved by Gopinath and co-workers,<sup>[54]</sup> Pettes co-workers,<sup>[37]</sup> and Dunn and co-workers.<sup>[41]</sup> Furthermore, after most of the Mo<sup>4+</sup> and Mo<sup>5+</sup> were transformed into Mo<sup>6+</sup>, bringing about the lattice ordering and blockage of the catalytic sites. It became difficult for the negatively charged sulfite to occupy the vacancy sites of A-MoO<sub>3-x</sub> which endows the reduced substrate capture ability and catalytic activity. This observation further confirmed the vacancy-engineered structure may play a crucial role for enhancing the SuO<sub>x</sub>-like activity of P-MoO<sub>3-x</sub> NPs.

Since the stability of enzymes is a vital factor for practical application, nanomaterials with enzyme-mimic activity are expected to be stable after long-term reaction. To prove this, the catalytic activities of P-MoO<sub>3-x</sub> NPs were measured for successive three cycles. After each cycle, P-MoO<sub>3-x</sub> NPs were washed for several times and collected by centrifugation before reused. As shown in Figure 5a, the SuO<sub>x</sub>-like activity shows negligible changed. Besides, it still maintains 91.92% after the third run which demonstrating the excellent stability of P-MoO<sub>3-x</sub> NPs for mimicking the SuO<sub>x</sub> enzyme (Figure 5b). In addition, the recycling measurements did not induce distinct difference of XRD (Figure S16, Supporting Information) or XPS patterns (Figure S17, Supporting Information), further confirms the stability of P-MoO<sub>3-x</sub> NPs.

As an artificial enzyme with intrinsic SuO<sub>x</sub> mimetic activity, P-MoO<sub>3-x</sub> NPs could catalyze the oxidation of sulfite to sulfate using K<sub>3</sub>[Fe (CN)<sub>6</sub>] as electron acceptor with the reduction of the absorbance at 420 nm. Generally, reductive sulfite was regarded to cause the irreversible cleavage of VB1.<sup>[29,55]</sup> Besides, VB1 was easier to bind with P-MoO<sub>3-x</sub> NPs via electrostatic reaction in comparison with sulfite. Therefore, VB1 was considered to inhibit the SuO<sub>x</sub>-like activity if P-MoO<sub>3-x</sub> NPs-sulfite-K<sub>3</sub>[Fe (CN)<sub>6</sub>] system with a change of color, which suggested the indirectly determination of VB1. Based on the inhibition of SuO<sub>x</sub>-like activity of P-MoO<sub>3-x</sub> NPs by VB1, a method for VB1 detecting has been proposed.

As shown in Figure 6a, the Δabsorbance versus time at 420 nm was gradually decreased after incubation with an increasing concentration of VB1. The velocity of the catalytic reaction versus VB1 concentration was significantly reduced, confirming the suppressed effect of VB1 (Figure 6b). Moreover, the concentration of detectable VB1 was 0.67 μg mL<sup>-1</sup> with a good linear range within 0.67–202.38 μg mL<sup>-1</sup> (0.2–600 × 10<sup>-3</sup> M, R<sup>2</sup> = 0.997). The limit of detection (LOD, S/N = 3)<sup>[25,50,56]</sup> for VB1 was 0.46 μg mL<sup>-1</sup>. Despite various analytic techniques have been carried out for the detection of VB1, such as high performance liquid chromatography (HPLC),<sup>[57]</sup> spectrofluorimetric,<sup>[58,59]</sup> and electrochemical methods,<sup>[60]</sup> the unstable signal, complicated and high cost of operation limit

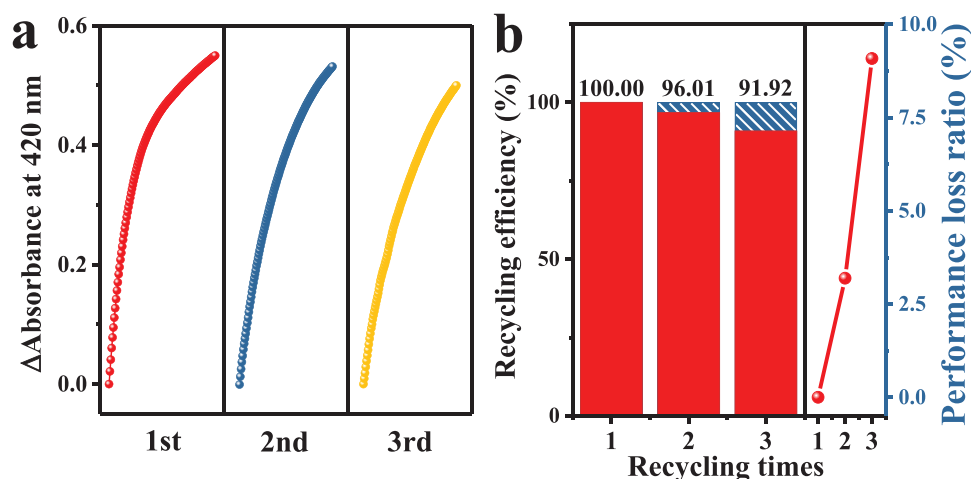
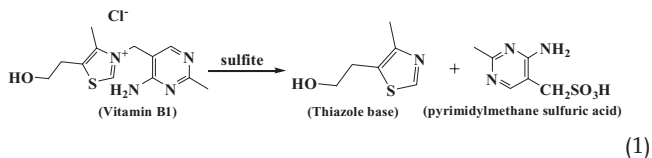


**Figure 5.** The stability of P-MoO<sub>3-x</sub> NPs. a) Recycling SuO<sub>x</sub>-like catalytic test of P-MoO<sub>3-x</sub> NPs after three continuous cycles. b) The performance loss ratio of P-MoO<sub>3-x</sub> NPs after three cycles.

their practical applications. In comparison with the reported procedure by different techniques or nanomaterials in Table S5 in the Supporting Information,<sup>[11,26,56,61,62]</sup> the LOD of this work has the same order of magnitude as those for carbon nanotubes (LOD = 0.44 μg mL<sup>-1</sup>) and Au-GQDs (LOD = 0.16 μg mL<sup>-1</sup>) which possess the most sensitive behavior so far from the literatures. Meanwhile, a wide range of VB1 could be detected by this approach, suggesting the excellent tolerance of this procedure in the environment with high concentration of VB1.

In addition, the detection mechanism was also investigated. In model systems as reported, VB1 was easily got cleaved through an irreversible base-exchange reaction or a nucleophilic displacement on the methylene group in which sulfite was regarded as the displacing base.<sup>[63]</sup> Meanwhile, as VB1 was gradually cleaved by reductive sulfite with the production of free thiazole base and pyrimidylmethane sulfuric acid,<sup>[29]</sup> it became inactivated. The reaction could be described as Equation (1). Hence, the addition of VB1 could effectively consumed sulfite absorbed on the surface of P-MoO<sub>3-x</sub> NPs resulting in the hindrance of SuO<sub>x</sub> activity.



Furthermore, zeta potential measurements were also employed to elucidate the mechanism of the above colorimetric assay (Figure 6c). P-MoO<sub>3-x</sub> NPs show a zeta potential value of -36.67 mV in the reaction solution, the value was decreased to -26.27 mV after the addition of positively charged VB1 (the zeta potential of VB1 alone was +7.6 mV). The reduction of the zeta potential value indicated the occurrence of electrostatic interaction between VB1 and the surface of P-MoO<sub>3-x</sub> NPs,<sup>[26]</sup> resulting in surface charge neutralization with the particle agglomeration.<sup>[64]</sup> This phenomenon was also confirmed by

TEM analysis (Figure S18, Supporting Information). The occurrence of particle agglomeration endows with the blockage of the catalytic sites. Moreover, the sulfite capture ability of P-MoO<sub>3-x</sub> NPs significantly decreased which would cause the hindrance of SuO<sub>x</sub> activity. These results suggested that VB1 could effectively attenuate the SuO<sub>x</sub> activity of P-MoO<sub>3-x</sub> NPs through two methods, first is the cleavage reaction of VB1 by sulfite, and the other is the electrostatic interaction between VB1 and P-MoO<sub>3-x</sub> NPs. The mechanism of the detecting approach was also represented in Figure 5e.

In addition, to further investigate the selectivity of P-MoO<sub>3-x</sub> NPs towards VB1, relevant Vitamin complex such as Vitamin C, other amino acid with thiol side chain or routine drugs were also tested (Figure 6d). The results show that responses for other additives were negligible, suggesting the good selectivity towards VB1 of this procedure.

### 3. Conclusion

In summary, we have demonstrated that hydrophilic P-MoO<sub>3-x</sub> NPs with abundant oxygen vacancies created by vacancy-engineering exhibit a level of SuO<sub>x</sub>-like activity 12 times higher than SuO<sub>x</sub>-like activity versus b-MoO<sub>3</sub> and could catalyze the oxidation of sulfite to sulfate. The oxygen vacancies were regarded as catalytic hotspots which allow better sulfite capture ability, resulting in an enhanced SuO<sub>x</sub> activity. Moreover, as the existence of VB1 would inhibit the SuO<sub>x</sub> mimic activity of P-MoO<sub>3-x</sub> NPs through the irreversible cleavage of VB1 by sulfite and the electrostatic interaction between VB1 and P-MoO<sub>3-x</sub> NPs, a colorimetric platform based on the SuO<sub>x</sub>-like activity of P-MoO<sub>3-x</sub> NPs which exhibits high sensitivity (LOD = 0.46 μg mL<sup>-1</sup>, linear relationship range from 0.67 to 202.38 μg mL<sup>-1</sup>) and good selectivity was first constructed for detecting VB1. This study utilized the biocatalytic behavior of P-MoO<sub>3-x</sub> NPs with intrinsic SuO<sub>x</sub> mimic activity for bio-sensing which may also lay the basis for further investigating the potential application of P-MoO<sub>3-x</sub> NPs via its SuO<sub>x</sub> mimic activity.



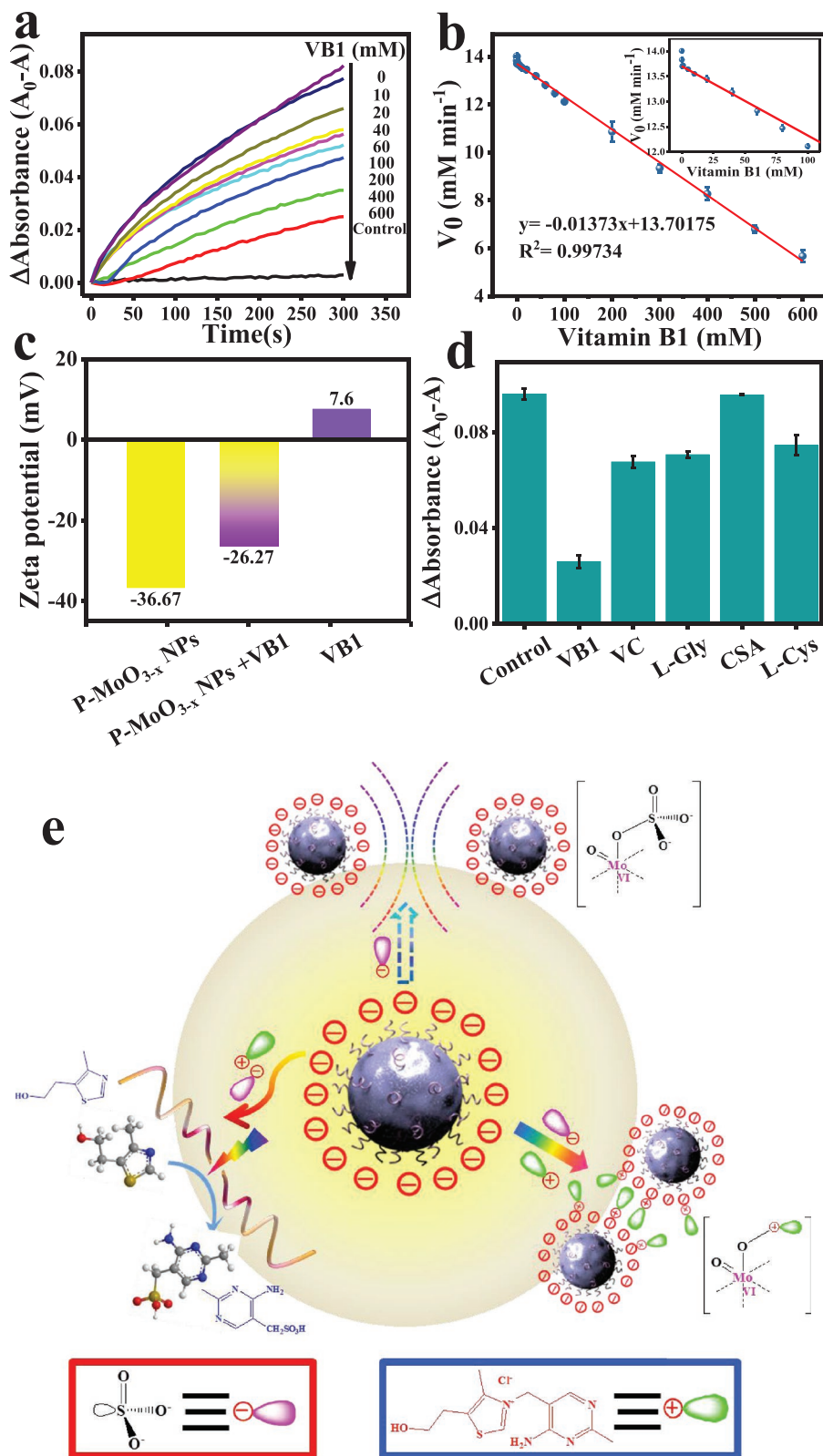


**Figure 6.** Detection of Vitamin B1 based on the  $\text{SuO}_x$ -like activity of  $\text{P-MoO}_{3-x}$  NPs. a) Time-dependent  $\Delta\text{Absorbance}$  ( $A_0-A$ ) at 420 nm of  $\text{P-MoO}_{3-x}$  NPs in the presence of increased concentrations of VB1. b) Concentration dependence of the  $\text{SuO}_x$ -like activity of  $\text{P-MoO}_{3-x}$  NPs in the presence of increased concentrations of VB1. Inset: the  $\text{SuO}_x$ -like activity of  $\text{P-MoO}_{3-x}$  NPs in low concentration level. The concentrations of sulfite and  $\text{K}_3[\text{Fe}(\text{CN})_6]$  in the assay were  $0.66$  and  $0.3 \times 10^{-3}$  M, respectively. c) The proposed mechanism of  $\text{P-MoO}_{3-x}$  NPs for VB1 detection through two approaches. First is the irreversible cleavage reaction between VB1 and substrate (sulfite). The other is the occurrence of electrostatic interaction between VB1 and the surface of  $\text{P-MoO}_{3-x}$  NPs.

## Supporting Information

Supporting Information is available from the Wiley Online Library or from the author.

## Acknowledgements

The National Basic Research Program of China (2014CB931700) and State Key Laboratory of Optoelectronic Materials and Technologies supported this work.

## Conflict of Interest

The authors declare no conflict of interest.

## Keywords

oxygen vacancy-engineered, P-MoO<sub>3-x</sub> NPs, sulfite oxidase mimetic, vitamin B1 detection

Received: June 18, 2019  
Revised: September 17, 2019  
Published online:

- [1] R. M. Garrett, J. L. Johnson, T. N. Graf, A. Feigenbaum, K. V. Rajagopalan, *Proc. Natl. Acad. Sci. USA* **1998**, *95*, 6394.
- [2] H. Schindelin, C. Kisker, K. V. Rajagopalan, *Adv. Protein Chem.* **2001**, *58*, 47.
- [3] A. Ahmad, S. Alimad, M. A. Baig, *J. Microbiol. Biotechnol.* **2008**, *18*, 379.
- [4] R. Ragg, F. Natalio, M. N. Tahir, H. Janssen, A. Kashyap, D. Strand, W. Tremel, *ACS Nano* **2014**, *8*, 5182.
- [5] M. Velayutham, C. F. Hemann, A. J. Cardounel, J. L. Zweier, *Biochem. Biophys. Rep.* **2016**, *5*, 96.
- [6] E. Karakas, H. L. Wilson, T. N. Graf, S. Xiang, S. Jaramillo-Busquets, K. V. Rajagopalan, *J. Biol. Chem.* **2005**, *280*, 33506.
- [7] J. O. Sass, A. Gunduz, C. A. R. Funayama; B. Korkmaz, K. G. D. Pinto, B. Tuysuz, L. Y. Dos Santos, E. Taskiran, M. de Fátima Turcato, C.-W. Lam, J. Reiss, M. Walter, C. Yalcinkaya, J. S. Camelo Junior, *Brain Dev.* **2010**, *32*, 544.
- [8] G. L. Arnold, C. L. Greene, J. P. Stout, S. I. Goodman, *J. Pediatr.* **1993**, *123*, 595.
- [9] P. S. Bindu, R. Christopher, A. Mahadevan, R. D. Bharath, *J. Child Neurol.* **2011**, *26*, 1036.
- [10] J. L. Johnson, *Prenatal Diag.* **2003**, *23*, 6.
- [11] H. J. Cohen, I. Fridovich, K. V. Rajagopalan, *J. Biol. Chem.* **1971**, *246*, 374.
- [12] S. Groysman, R. H. Holm, *Biochemistry* **2009**, *48*, 2310.
- [13] Z. G. Xiao, C. G. Young, J. H. Enemark, A. G. Wedd, *J. Am. Chem. Soc.* **1992**, *114*, 9194.
- [14] S. K. Das, P. K. Chaudhury, D. Biswas; S. Sarkar, *J. Am. Chem. Soc.* **1994**, *116*, 9061.
- [15] M. P. Coughlan, *Molybdenum and Molybdenum-Containing Enzymes*, Elsevier Science, Amsterdam, Netherlands **2014**.
- [16] J. J. X. Wu, X. Wang, Q. Wang, Z. P. Lou, S. R. Li, Y. Y. Zhu, L. Qin, H. Wei, *Chem. Soc. Rev.* **2019**, *48*, 1004.
- [17] H. Wei, E. Wang, *Chem. Soc. Rev.* **2013**, *42*, 6060.
- [18] N. J. Lawrence, J. R. Brewer, L. Wang, T. S. Wu, J. Wells-Kingsbury, M. M. Ihrig, G. H. Wang, Y. L. Soo, W. N. Mei, C. L. Cheung, *Nano Lett.* **2011**, *11*, 2666.
- [19] A. A. Vernekar, T. Das, G. Mugesh, *Angew. Chem.* **2016**, *128*, 1434.
- [20] E. G. Heckert, A. S. Karakoti, S. Seal, W. T. Self, *Biomaterials* **2008**, *29*, 2705.
- [21] G. Pulido-Reyes, I. Rodea-Palomares, S. Das, T. S. Sakthivel, F. Leganes, R. Rosal, S. Seal, F. Fernández-Piñas, *Sci. Rep.* **2015**, *5*, 15613.
- [22] Z.-Y. Yang, S.-L. Luo, H. Li, S.-W. Dong, J. He, H. Jiang, R. Li, X.-C. Yang, *RSC Adv.* **2014**, *4*, 59965.
- [23] A. Leyva-Pérez, D. Cómbita-Merchán, J. R. Cabrero-Antonino, S. I. Al-Resayes, A. Corma, *ACS Catal.* **2013**, *3*, 250.
- [24] K. Herget, P. Hubach, S. Pusch, P. Deglmann, H. Götz, T. E. Gorelik, I. A. Gural'skiy, F. Pfitzner, T. Link, S. Schenk, M. Panthöfer, V. Ksenofontov, U. Kolb, T. Opatz, R. André, W. Tremel, *Adv. Mater.* **2017**, *29*, 1603823.
- [25] R. Rajamanikandan, M. Ilanchelian, *Sens. Actuators, B* **2017**, *244*, 380.
- [26] B. Sinduja, S. Abraham John, *New J. Chem.* **2019**, *43*, 2111.
- [27] S. Manzetti, J. Zhang, D. van der Spoel, *Biochemistry* **2014**, *53*, 821.
- [28] R. K. Gupta, S. K. Yadav, V. A. Saraswat, M. Rangan, A. Srivastava, A. Yadav, R. Trivedi, S. K. Yachha, R. K. S. Rathore, *Clin. Nutr.* **2012**, *31*, 422.
- [29] B. K. Dwivedi, R. G. Arnold, *J. Agric. Food Chem.* **1973**, *21*, 54.
- [30] W. Y. Yin, T. Bao, X. Zhang, Q. Gao, J. Yu, X. H. Dong, L. Yan, Z. J. Gu, Y. L. Zhao, *Nanoscale* **2018**, *10*, 1517.
- [31] C. Du, Q. Zhang, Z. Y. Lin, B. Yan, C. X. Xia, G. W. Yang, *Appl. Catal., B* **2019**, *248*, 193.
- [32] T. Bao, W. Y. Yin, X. P. Zheng, X. Zhang, J. Yu, X. H. Dong, Y. Yong, F. P. Gao, L. Yan, Z. J. Gu, Y. L. Zhao, *Biomaterials* **2016**, *76*, 11.
- [33] H. R. Zu, Y. X. Guo, H. Y. Yang, D. Huang, Z. M. Liu, Y. L. Liu, C. F. Hu, *New J. Chem.* **2018**, *42*, 18533.
- [34] Q. C. Lu, Y. Yang, J. R. Feng, X. Wang, *Sol. RRL* **2019**, *3*, 1800277.
- [35] D. D. Ding, W. C. Huang, C. Q. Song, M. Yan, C. S. Guo, S. Q. Liu, *Chem. Commun.* **2017**, *53*, 6744.
- [36] S. Yazdani, R. Kashfi-Sadabad, T. D. Huan, M. D. Morales-Acosta, M. T. Pettes, *Langmuir* **2018**, *34*, 6296.
- [37] R. Kashfi-Sadabad, S. Yazdani, T. D. Huan, Z. Cai, M. T. Pettes, *J. Phys. Chem. C* **2018**, *122*, 18212.
- [38] J. Cao, W. S. Nie, L. Huang, Y. B. Ding, K. L. Lv, H. P. Tang, *Appl. Catal., B* **2019**, *241*, 18.
- [39] G. H. Dong, W. K. Ho, C. Y. Wang, *J. Mater. Chem. A* **2015**, *3*, 23435.
- [40] J. S. Zhang, M. W. Zhang, R.-Q. Sun, X. C. Wang, *Angew. Chem., Int. Ed.* **2012**, *51*, 10145.
- [41] H. S. Kim, J. B. Cook, H. Lin, J. S. Ko, S. H. Tolbert, V. Ozolins, B. Dunn, *Nat. Mater.* **2017**, *16*, 454.
- [42] V. Bhosle, A. Tiwari, J. Narayan, *J. Appl. Phys.* **2005**, *97*, 083539.
- [43] J. J. Zhang, Y. M. Pan, Y. F. Chen, H. B. Lu, *J. Mater. Chem. C* **2018**, *6*, 2216.
- [44] P. Kalimuthu, A. A. Belaidi, G. Schwarz, P. V. Bernhardt, *J. Phys. Chem. B* **2017**, *121*, 9149.
- [45] H. J. Cohen, I. Fridovich, K. V. Rajagopalan, *J. Biol. Chem.* **1971**, *246*, 359.
- [46] L. Z. Gao, J. Zhuang, L. Nie, J. B. Zhang, Y. Zhang, N. Gu, T. H. Wang, J. Feng, D. L. Yang, S. Perrett, X. Y. Yan, *Nat. Nanotechnol.* **2007**, *2*, 577.
- [47] W. B. Shi, Q. T. Wang, Y. J. Long, Z. L. Cheng, S. H. Chen, H. Z. Zheng, Y. M. Huang, *Chem. Commun.* **2011**, *47*, 6695.
- [48] K. R. Hoke, N. Cobb, F. A. Armstrong, R. Hille, *Biochemistry* **2004**, *43*, 1667.
- [49] T. M. Chen, X. J. Wu, J. X. Wang, G. W. Yang, *Nanoscale* **2017**, *9*, 11806.
- [50] Y. Chen, T. M. Chen, X. J. Wu, G. W. Yang, *Sens. Actuators, B* **2019**, *279*, 374.

- [51] K. Chen, A. Bayaguud, H. Li, Y. Chu, H. C. Zhang, H. L. Jia, B. F. Zhang, Z. C. Xiao, P. F. Wu, T. B. Liu, Y. G. Wei, *Nano Res.* **2018**, *11*, 1313.
- [52] M. R. He, R. N. Zhang, K. Zhang, Y. N. Liu, Y. L. Su, Z. Y. Jiang, *J. Mater. Chem. A* **2019**, *7*, 11468.
- [53] H. F. Cheng, T. Kamegawa, K. Mori, H. Yamashita, *Angew. Chem., Int. Ed.* **2014**, *53*, 2910.
- [54] K. P. Reddy, N. B. Mhamane, M. K. Ghosalya, C. S. Gopinath, *J. Phys. Chem. C* **2018**, *122*, 23034.
- [55] R. R. Williams, R. E. Waterman, J. C. Keresztesy, E. R. Buchman, *J. Am. Chem. Soc.* **1935**, *57*, 536.
- [56] P. K. Brahman, R. A. Dar, K. S. Pitre, *Sens. Actuators, B* **2013**, *177*, 807.
- [57] J. Tan, R. Li, Z.-T. Jiang, *Anal. Methods* **2011**, *3*, 1568.
- [58] Y. Li, P. Wang, X. Wang, M. Cao, Y. S. Xia, C. Cao, M. G. Liu, C. Q. Zhu, *Microchim. Acta* **2010**, *169*, 65.
- [59] J. F. Sun, L. H. Liu, C. L. Ren, X. G. Chen, Z. D. Hu, *Microchim. Acta* **2008**, *163*, 271.
- [60] Q. Wan, N. Yang, Y. Ye, *Anal. Sci.* **2002**, *18*, 413.
- [61] R. Purbia, S. Paria, *ACS Appl. Nano Mater.* **2018**, *1*, 1236.
- [62] H. B. Li, F. Chen, *J. Sep. Sci.* **2001**, *24*, 271.
- [63] C. H. Suelter, D. E. Metzler, *Bioch. Biophys. Acta* **1960**, *44*, 23.
- [64] A. Vujačić, V. Vodnik, S. P. Sovilj, M. Dramićanin, N. Biblić, S. Milonjć, V. Vasić, *New J. Chem.* **2013**, *37*, 743.